Advances in Geo-Energy Research

Vol. 2, No. 2, p. 173-189, 2018
www.astp-agr.com

Original article

Thermo-Hydro-Mechanical-Chemical processes in geological disposal of radioactive waste – An example of regulatory research

Thanh Son Nguyen*

Canadian Nuclear Safety Commission, Ottawa, Canada

(Received March 5, 2018; revised March 19, 2018; accepted March 21, 2018; available online March 26, 2018)

Citation:
Nguyen, T.S.
Thermo-Hydro-Mechanical-Chemical processes in geological disposal of radioactive waste – An example of regulatory research. *Advances in Geo-Energy Research,* 2018, 2(2): 173-189, doi: 10.26804/ager.2018.02.06.

Corresponding author:
*E-mail: son.nguyen@canada.ca

Keywords:
Radioactive wastes
geological disposal
coupled processes

Abstract:
Deep geological disposal is being considered in Canada and many other countries as the most viable option for the long-term management of radioactive waste. The disposal method consists of emplacing the waste in a repository built at hundreds of metres depth in a suitable host rock. A multi-barrier system, that includes the host rock formation as a major component, would be provided in order to protect humans and the environment from the harmful effects of the waste for very extensive time periods. Many events and processes are expected to occur during the lifetime of the repository, such as heat generation from the waste, seismicity and glaciation. As a result of those events and processes the Thermal-Hydraulic-Mechanical-Chemical (THMC) regimes in the natural and engineered components of the multi-barrier system will be perturbed, and the evolution of the THMC regimes and how this evolution affects the multi-barrier performance need to be understood. The Canadian Nuclear Safety Commission (CNSC), Canada's nuclear regulator, has been conducting independent experimental and theoretical research on coupled THMC processes for several decades. As part of this research, the CNSC used experimental data from laboratory tests and large-scale experiments at underground research laboratories (URL) in order to develop a mathematical framework for the simulation of coupled processes in engineered and natural barriers for geological disposal. In this paper, we describe that mathematical framework and show examples of how it was adapted and applied to several situations: water and gas injection experiment at an URL, a heater experiment at an URL, and the effects of nine glacial cycles in a sedimentary rock formation.

1. Introduction

Geological disposal of radioactive waste originating from the production of electricity is being considered in many countries, including Canada. A deep geological repository (DGR) relies on a system of multiple engineered and natural barriers in order to provide long-term containment and isolation of the highly radioactive used fuel, in order to protect people and the environment for very long periods of time. During the very long time period after closure of the DGR, the multiple barrier system will be subject to perturbations that result in coupled thermo-hydro-mechanical-chemical (THMC) processes that would affect the long-term performance of the barriers.

In Canada, the Nuclear Waste Management Organization (NWMO) is the implementer of the geological disposal project for Canada's used nuclear fuel, and is currently performing site selection among volunteer communities in the province of Ontario. The Canadian Nuclear Safety Commission (CNSC), the nuclear regulator in Canada, will ultimately be responsible for the licensing of a DGR. Following international best practice, the CNSC is building a solid objective knowledge base through a program of independent research in order to support future licensing decisions and regulatory oversight should the DGR project be proposed, accepted and implemented in the future. This paper presents the CNSC research on coupled THMC processes which have important implications on the long-term safety of a DGR.

2. The multiple barrier concept for geological disposal of radioactive waste

The current Canadian concept for geological disposal of used nuclear fuel (Noronha, 2016), similar to international concepts, consists of burying the used fuel at depths of hundreds of metres in a system of emplacement rooms excavated in a suitable rock formation. The safety of the DGR system must be ensured for hundreds of thousands to millions of years

https://doi.org/10.26804/ager.2018.02.06.

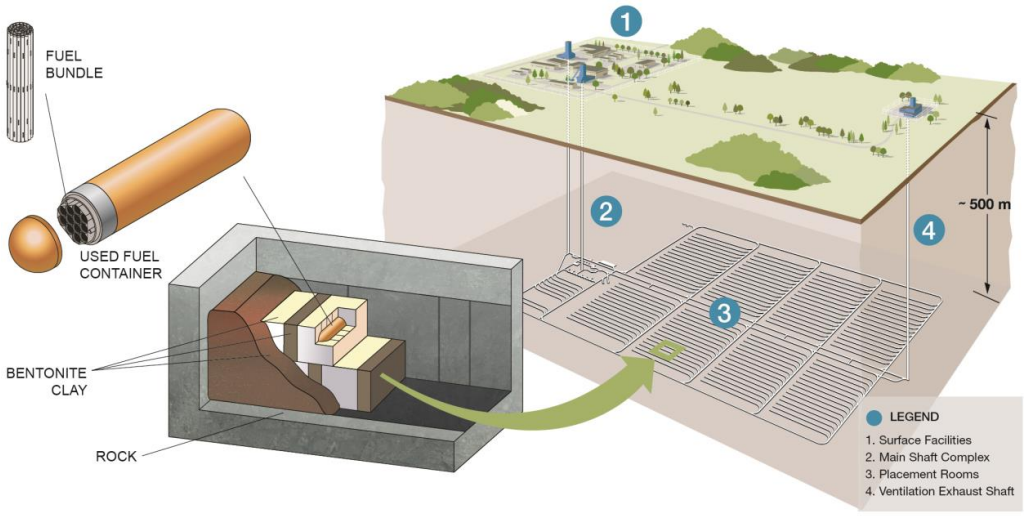

Fig. 1. Current Canadian concept of geological disposal (from Noronha, 2016).

in order to protect humans and the environment for such long periods of time. Fig. 1 shows the current Canadian concept. It shows that long-term safety is provided by a system of multiple, redundant barriers that will contain the wastes and isolate them from the near surface environment. The first barrier is the nuclear fuel pellet that is durable and temperature-resistant, and possesses a low dissolution potential. The second barrier is the fuel elements and bundles. A bundle is composed of a number of sealed tubes called elements, in which the fuel pellets are inserted. The fuel elements are made of corrosion-resistant zircaloy. The third barrier is the fuel container which is designed to be resistant to anticipated loads and corrosion. Each container will contain 48 fuel bundles. The fourth barrier is a compacted bentonite sealing system that would surround the container in the emplacement room. The fifth barrier is the natural rock formations that will protect the DGR from natural events and from human intrusion, and also provide a barrier to eventual radionuclide migration to the near surface.

It is expected that during the very long time frame after closure of the DGR, the multiple barrier system will be subject to perturbations that will affect its long-term performance and its safety functions. Those perturbations include excavation of the emplacement rooms and shafts of the DGR, heat generated from the waste, gas generated from corrosion products and organics that might be present in the DGR, and geological events such as glaciation and seismicity. Those perturbations disrupt the existing equilibrium of the engineered and natural barriers by inducing THMC processes that are in general mutually coupled. The long-term performance of the barriers will be affected by coupled THMC processes, and therefore the understanding of the processes through experimental and theoretical research is necessary in order to assess the long-term safety of the DGR system. Since the early 1990s, the CNSC has been collaborating with Canadian and international partners to conduct research on coupled THMC processes. Experimental data were generated from small-scale experiments performed in conventional surface laboratories, larger scale experiments from underground research laboratories, and geological scale data from paleohydrogeological information. The experimental data provide the basis for the development of a mathematical framework of coupled THMC processes. In this paper, the general mathematical framework and the resulting mathematical model developed by the CNSC will be discussed. Examples on how the mathematical model was adapted to simulate different situations where coupled THMC processes prevail will be presented.

3. Conceptualization of coupled THMC processes

The CNSC has developed conceptual and mathematical models for coupled THMC processes since the early 1990s. Following Tsang (1987), coupled processes in geological media could be illustrated by the interaction diagram shown in Fig. 2.

It is commonly assumed that the geological medium can be idealized as a porous medium, comprised of an assemblage of solid particles, the solid skeleton. The solid assemblage is pervaded by discontinuities such as pores, cracks and microcracks. These discontinuities, which we will simply refer to as pores, can be filled by several types of fluids, in gaseous or liquid states. Referring to Fig. 2, let us look at the different interaction vectors, as follows:

- T->M: A change in temperature induces thermal expansion and contraction in the soil skeleton, leading to thermal stresses if deformations are constrained.
- T->H: An increase in temperature induces thermal expansion of the pore fluids, leading to an increase in pore fluid pressures if drainage away from the heat source is impeded.
- H->T: Flow of pore fluids is responsible for heat transfer

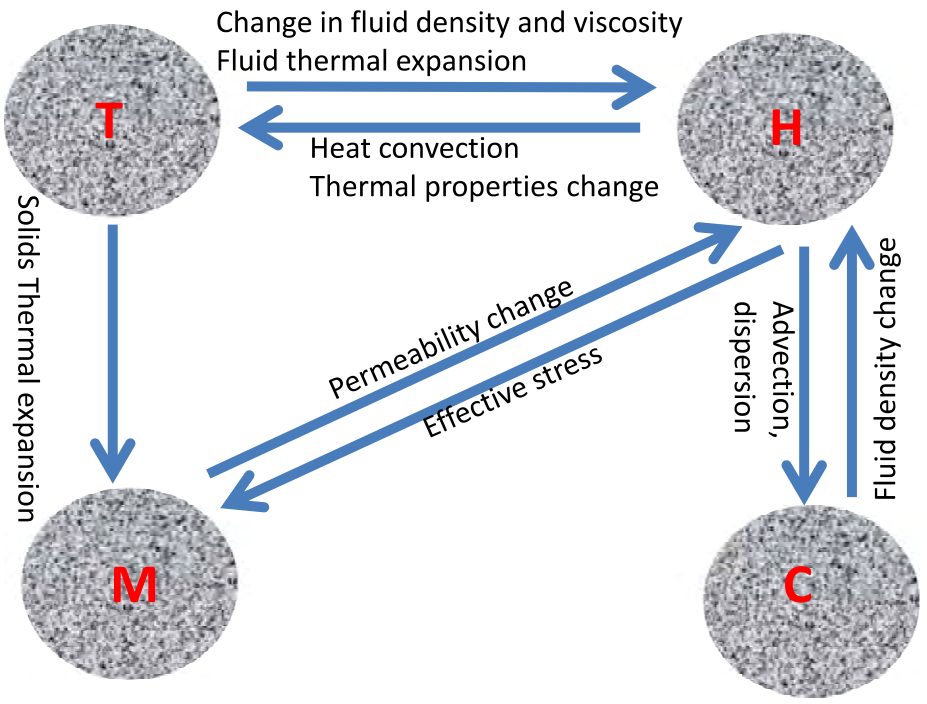

Fig. 2. Possible interaction for THMC processes around deep geological repositories.

by convection. Heat convection can usually be neglected in very low permeability formations. In media partially saturated with water, resaturation from infiltrating water can increase the bulk thermal conductivity and heat capacity.

- H->M: When external loads are applied on the porous medium, a new state of stress will develop. This total stress will be distributed among the solid skeleton and the pore fluids. We used and adapted the classical effective stress principle (Terzaghi, 1923; Biot, 1941; Bishop and Blight, 1963) in order to take into account that distribution, as detailed later in this paper.
- M->H: Deformation of the solid skeleton will change the pore volume that could be irreversible depending on the stress level, and consequently will affect the permeability of the medium.
- H->C: When solutes or radionuclides are present in the pore fluid, they can migrate by advection, dispersion and diffusion.
- C->H: Solutes can change the density of water. In some sedimentary rock formations in Canada, the porewater is a brine, with total dissolved solids (TDS) concentration of the order of hundreds of g/L, and density of up to 1.3 g/L.

The mathematical formulation of the above processes are based on the basic principle of conservation of mass and energy, quasi-static equilibrium of the solid skeleton, together with the adoption of the effective stress principle and constitutive relations governing the stress-strain behaviour of the solid skeleton, and the fluxes of mass and energy.

The above general formulation has been applied to many studies related to geological disposal of radioactive wastes. Based on that formulation, mathematical models were developed and implemented into computer codes. Since 1992, an international collaborative project called DECOVALEX (www.decovalex.org) has gathered researchers to develop coupled THMC models, perform model inter-comparison, and validate the models with field and laboratory experiments. As a participant in DECOVALEX, the CNSC has developed and validated THMC models. Additionally the CNSC also focuses on the implications of coupled THMC processes on safety aspects related to the geological disposal of radioactive waste (Selvadurai and Nguyen, 1996; Nguyen et al., 2005; Nguyen et al., 2009; Nasir et al., 2012; Le and Nguyen, 2014; Nguyen and Le, 2014, 2015; Nasir et al., 2017; Nguyen and Li, 2017). The objective of this paper is not to provide a comprehensive review of all research endeavours in coupled THMC, within or outside of the DECOVALEX project. Instead, the author focuses on our recent contributions in that area of research, and from the results strive to identify specific implications on the design and safety assessment of a DGR. The mathematical formulation and results from the following examples will be discussed:

- The simulation of a heater experiment in an argillaceous rock formation.
- The simulation of gas and water migration in an argillaceous rock formation.
- The THMC response of a sedimentary rock basin to continental glaciation.

4. Heater experiment in an argillaceous rock formation

The Mont Terri Underground Research Laboratory (URL),

in Switzerland, is sited in a clay/shale formation called Opalinus Clay (OPA). This rock formation is being considered as a candidate formation for geological disposal of radioactive wastes in Switzerland. Many experiments are being and have been performed at Mont-Terri in order to characterize and further understand the hydrogeological, mechanical and geochemical behaviour of OPA. The HE-D experiment is one such experiment that took place in 2004-2005 (Wileveau, 2005). The HE-D experiment simulates the effects of radiogenic heat from a waste container on the THM regime in the near field rock. The experiment consisted of drilling a 30 cm diameter borehole into the OPA, in which two heating devices were emplaced. Power injection to both heaters was performed in two stages. In stage 1, the total power injected to both heaters was maintained at 650 W from April 6, 2004 to July 7, 2004. In stage 2, that power was rapidly raised to 1950 W and maintained at that level until May 11, 2005 at which time the power was interrupted. Many monitoring boreholes exist in the vicinity of the micro-tunnel. These are equipped with sensors that measure temperatures, porewater pressures and deformations of the rock mass before, during and after heating.

4.1 Governing equations

In order to simulate the THM response of the rock mass in the HE-D experiment, we conceptualize it as a saturated porous medium. When heat is injected in that medium, it raises the ambient temperature. The increase in temperature results in a tendency for thermal expansion in the solid phase, the solid skeleton and the pore fluid. The temperature transient triggers an increase in the pore fluid pressure that will dissipate when drainage away from the heat source occurs. Using the methodology detailed above, the mathematical model consists of a system of partial differential equations, together with the applicable boundary and initial conditions. The equations are as follows:

$$\frac{\partial}{\partial x_i}\left(\kappa_{ij}\frac{\partial T}{\partial x_j}\right)+q=\rho C\frac{\partial T}{\partial t} \tag{1}$$

$$\frac{\partial}{\partial x_i}\left(\frac{\rho_w k_{ij}}{\mu}\left(\frac{\partial p}{\partial x_j}+\rho_w g j\right)\right)+\rho_w\left[\frac{-n}{K_w}+\frac{n-\alpha}{K_s}\right]\frac{\partial p}{\partial t}+\rho_w\alpha\frac{\partial}{\partial t}\left(\frac{\partial u_k}{\partial x_k}\right)+\rho_w\left((1-\alpha)\beta-n\beta_w-(1-n)\beta_s\right)\frac{\partial T}{\partial t}=0 \tag{2}$$

$$\frac{1}{2}C_{ijkl}\left(\frac{\partial^2 u_k}{\partial x_j\partial x_k}+\frac{\partial^2 u_l}{\partial x_i\partial x_l}\right)+\alpha\frac{\partial p}{\partial x_i}=0 \tag{3}$$

The primary unknowns of the above equations are: T, temperature; u_i, displacement of the solid skeleton; and p, pore pressure (the convention is for tension to be positive). These variables are functions of both the spatial variables (x_i) and time (t). A summary of the meaning and hypotheses used for each equation is given as follows:

a) Equation of heat conservation:

Eq. (1) was derived from the principle of heat conservation. It is assumed that heat conduction is the only mechanism of heat transport. κ_{ij} is the thermal conductivity tensor (W/m/C), ρ is the density of the bulk medium (kg/m^3), C is the bulk specific heat of the medium (J/kg/C) and q is a distributed heat source (W/m^3).

b) Equation of pore fluid flow:

Eq. (2) is derived from the consideration of mass conservation for the pore fluid.

- The first term of the equation results from the adoption of Darcy's law for pore fluid flow. In this term, k_{ij} is the saturated permeability tensor (m^2); μ (kg/m/s) is the viscosity of the pore fluid; ρ_w is the density of the pore fluid; and g_i is the vector of the acceleration due to gravity. Both viscosity and density are temperature-dependent.
- The second term is a storage term coming from considerations of compressibility of the water and the solid phase, where K_w is the bulk modulus of the pore fluid (Pa) and K_s is the bulk modulus of the solid phase (Pa).
- The third term is a storage term originating from the consideration of compressibility of the porous skeleton.
- The fourth term represents water flow induced by thermal expansion of the pore fluid and the solid material, where β_w and β_s (1/°C) are the coefficient of volumetric thermal expansion of the water of the solid material, respectively.

c) Equation of equilibrium:

Eq. (3) is derived from the principle of pseudo-static equilibrium of the porous medium. In this equation, C_{ijkl} is the stiffness tensor that relates stress to strain; β is the coefficient of volumetric thermal expansion of the solid skeleton; and α is Biot's coefficient.

4.2 Numerical simulation and results

In this simulation, we assumed that the OPA is a transversely isotropic elastic medium, with principal directions that are parallel and perpendicular to the bedding orientation. The governing Eqs. (1)-(3) with assumed initial and boundary conditions were solved numerically using the finite method. The finite element representation with the corresponding initial and boundary conditions are illustrated in Fig. 3. The bedding planes orientation (at approximately 45^o with respect to the horizontal) is also illustrated in Fig. 3. The hydraulic and mechanical properties must reflect the presence of bedding. The THM properties used for input to the model are derived from the range of values suggested in Wileveau (2005) and are shown in Table 1.

The calculated temperature and pore pressure fields at one point in time of the second heating cycle are shown in Fig. 4. The ellipsoidal shape of both fields in cross sections perpendicular to the heaters is a direct consequence of the assumption of transverse isotropy for both thermal and flow processes. Fig. 5 shows the temperature and pore pressure evolution for several points located around the heaters. It can be seen that the calculated results are in excellent agreement

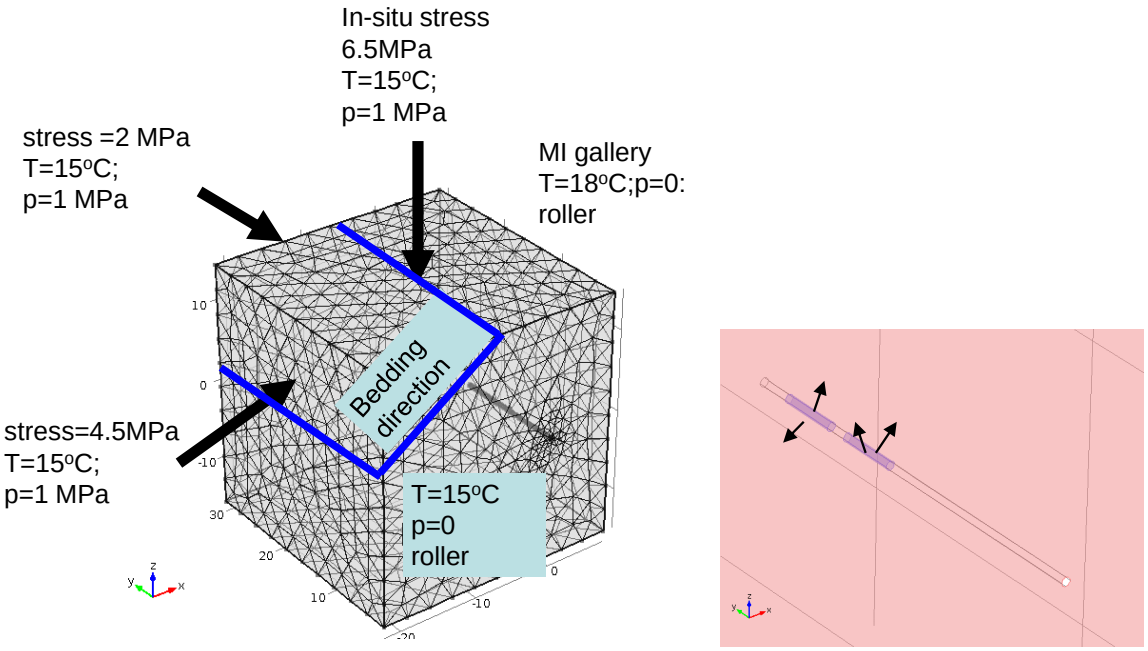

(a) Entire model

(b) Radial heat flux from heaters

Fig. 3. Finite element model of the HE-D heater experiment.

Table 1. Input properties for heater experiment.

Initial conditions	Total stress (MPa)	σ_{xx}	4.5
		σ_{yy}	2
		σ_{zz}	6.5
	Porewater pressure (MPa)	p	1
	Temperature (°C)	T	15
Main parameters	Young's modulus in the bedding plane direction (*) (MPa)	E_h	8,000
	Young's modulus in perpendicular direction to bedding (*) (MPa)	E_v	3,000
	Poisson's ratio (*)	ν_{hh}	0.24
		ν_{vh}	0.33
	Shear modulus (*) (MPa)	G_{vh}	1,000
	Biot's coefficient	α	0.6
	Porosity	n	0.157
	Dry density (kg/m^3)	\	2,450
	Intrinsic permeability in bedding plane direction (m^2)	k_h	4×10^{-20}
	Anisotropy ratio-permeability	k_h/k_v	4
		$k_0 = (k_h k_h k_v)^{(1/3)}$	1.77
	Thermal conductivity (W/m/K)	\	1.8
		k_h/k_v	\
	Heat Capacity of solid (J/kg/°K)	\	800
	Linear solid thermal expansion coefficient (1/°K)	\	1.5×10^{-5}

(*) h: direction parallel to bedding; v: direction perpendicular to bedding

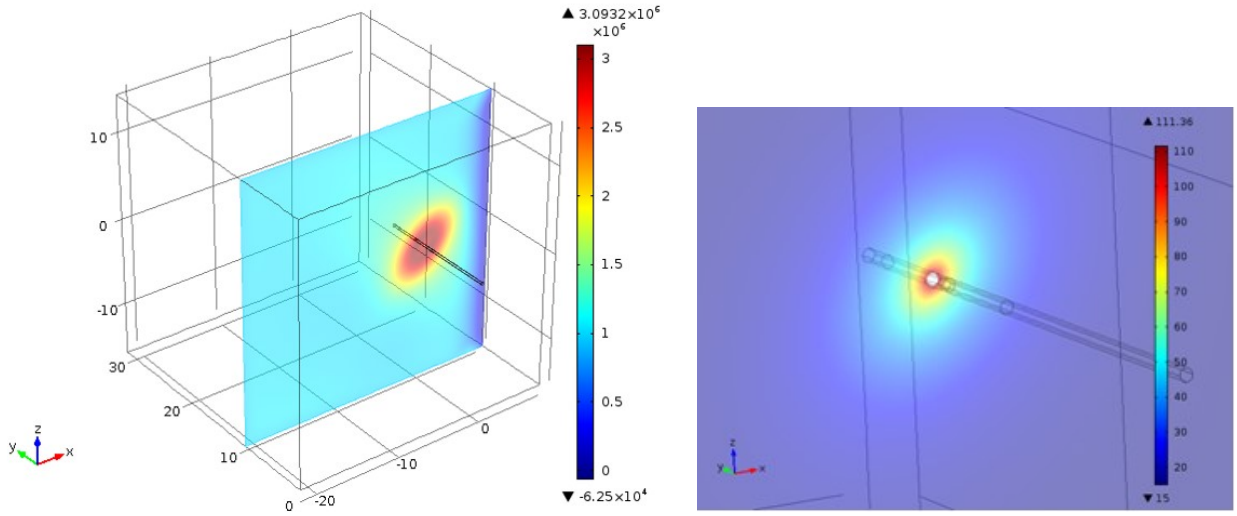

(a) Pressure (Pa) (b) Temperature (^{o}C)

Fig. 4. Temperature and pore pressure field.

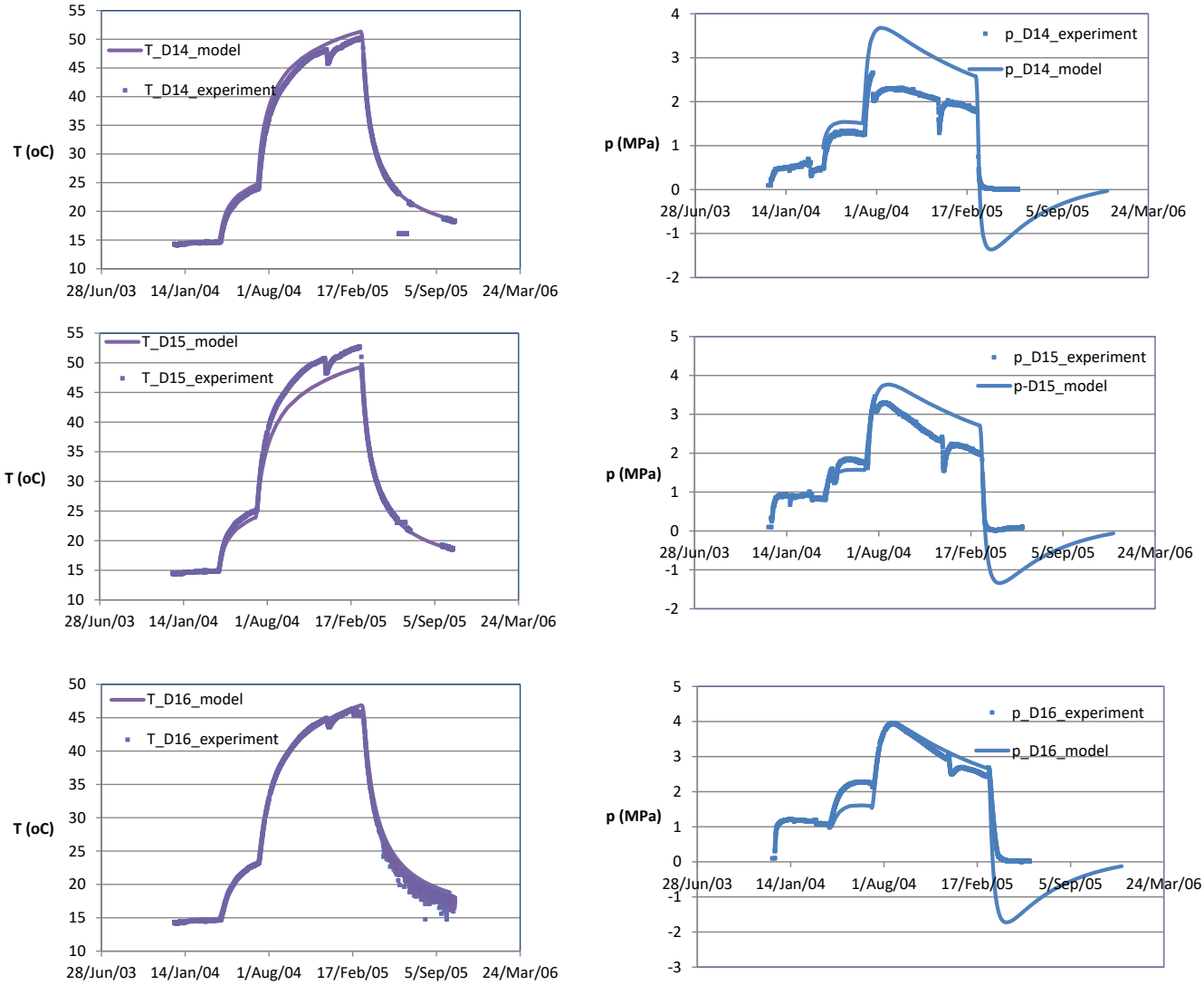

Fig. 5. Temperature and pressure variations – comparison between modelling results and measurements.

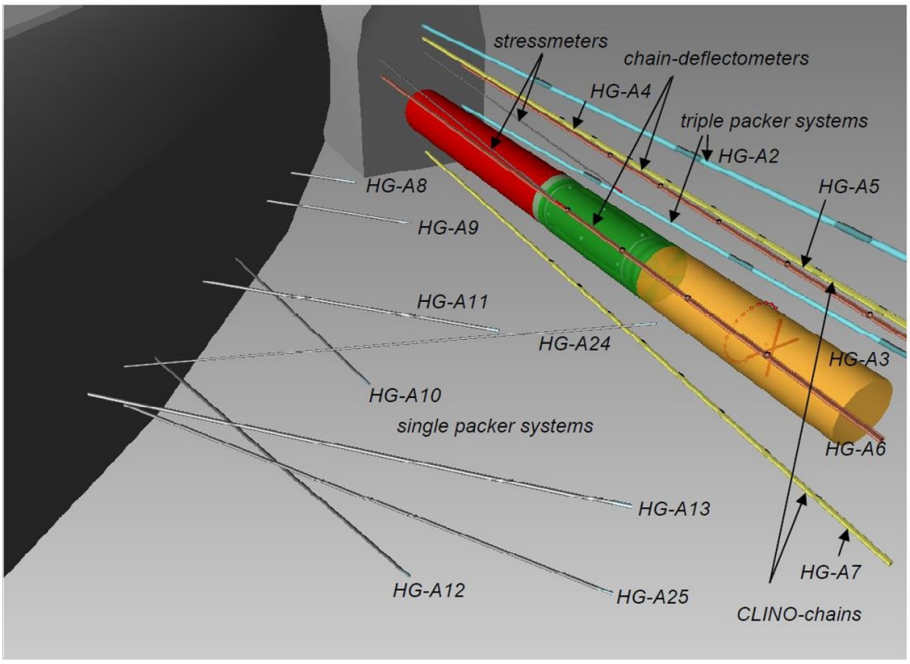

Fig. 6. HG-A experimental layout (from Marschall et al. 2008).

with the measured values. Each phase of heating induces a sharp increase in porewater pressure, followed by gradual decreases due to radial drainage away from the heat source while the temperature continues to increase due to the constant supply of heat. The rate of porewater decrease is a direct reflection of the permeability of the medium. The model is shown to be capable of predicting both qualitatively and quantitatively the above phenomena.

A high pore pressure can induce damage by hydrofracturing in intact rock, when it exceeds the minimum principal stress. In the HE-D experiment, hydrofracturing might have occurred at some points, since the measured pore pressure reached a maximum value of 4 MPa and is higher than the subhorizontal minimum principal stress estimated to be in the range of 2-3 MPa. Gens et al. (2007) indicated that the measured unconfined Young's moduli showed a decrease in value by a factor of six within 2 m of the heating boreholes, suggesting that the damage might extend to the same distance into the rock. When faults exist in the vicinity of a DGR, thermally induced pore pressure increase would decrease the effective normal stress and consequently the shear strength, potentially triggering fault re-activation in the extreme case. The thermally induced pore pressure in and around a DGR and its implications on safety should therefore be assessed.

5. Simultaneous gas and water flow in bedded argillaceous rocks

The large scale HG-A experiment investigates water and gas migration in the excavation damage zone (EDZ) and undisturbed host rock around a backfilled and sealed tunnel (Lanyon et al., 2010) at the Mont-Terri URL. The following activities were performed in sequence: tunnel excavation, tunnel backfilling and sealing, sealed tunnel section resaturation, water injection and gas injection. The hydro-mechanical regime of the rock mass was continually monitored. The experimental set-up is represented in Fig. 6. The tunnel is 13 m long and is 1.036 m in diameter. It is divided into three main sections: the liner section (0-6 m), the packer section (6-10 m) and the test section (10-13 m). Prior to excavation, 12 instrument boreholes were drilled. They were equipped with piezometers, deflectometer chains and inclinometer chains in order to continuously monitor the hydro-mechanical evolution of the rock in response to the activities of the experiment. A drilling machine was used to excavate the tunnel during an 8-day period. The bedding planes are oriented at approximately 45^{o} with respect to the horizontal direction and strike parallel to the axis of the tunnel. The test section at the end of the tunnel (Fig. 6) was filled with sand and gravel. A megapacker was emplaced and inflated to hydraulically isolate the test section from the rest of the microtunnel. The last two activities of the HG-A experiment consist of water injection, followed by gas injection in the test section of the tunnel. Piezometers were emplaced in the rock near the contact with the megapacker at three sections in order to measure pore pressure response due to water and gas injection. The piezometers were located at the 3, 6, 9 and 12 o'clock positions (looking towards the end of the tunnel).

5.1 Governing equations

The development of the governing equations of the model followed the general procedure described in section 3 and is detailed in Nguyen and Le (2014) and Le and Nguyen (2014). The equations are written in tensorial notation, as follows:

$$\frac{\partial}{\partial x_i}\left[\rho_g k_{ij}\left(\frac{k_{rg}}{\mu_g}\left(\frac{\partial p_g}{\partial x_j}+\rho_g g_j\right)+H\frac{k_{rw}}{\mu_w}\left(\frac{\partial p_w}{\partial x_j}+\rho_w g_j\right)\right)\right]$$
$$=\rho_g[n(H-1)\left(\frac{dS_w}{dp_c}\right)\frac{\partial p_c}{\partial t}+\frac{n(1-S_w+HS_w)}{K_g}\frac{\partial p_g}{\partial t}-$$
$$(1-S_w+HS_w)(\frac{n+\alpha_B}{K_s})\frac{\partial \bar{p}}{\partial t}+\alpha_B(1-S_w+HS_w)\frac{\partial^2 u_k}{\partial t\partial x_k} \quad (4)$$

$$\frac{\partial}{\partial x_i}\left[\rho_w k_{ij}\frac{k_{rw}}{\mu_w}\left(\frac{\partial p_w}{\partial x_j}+\rho_w g_j\right)\right]=\rho_w[n\left(\frac{dS_w}{dp_c}\right)\frac{\partial p_c}{\partial t}+ \quad (5)$$
$$\frac{nS_w}{K_w}\frac{\partial p_w}{\partial t}-S_w(\frac{n+\alpha_B}{K_s})\frac{\partial \bar{p}}{\partial t}+\alpha_B S_w\frac{\partial^2 u_k}{\partial t\partial x_k}]$$
$$\frac{1}{2}C_{ijkl}\left(\frac{\partial^2 u_k}{\partial x_j\partial x_k}+\frac{\partial^2 u_i}{\partial x_i\partial x_l}\right)+\alpha_B\frac{\partial \bar{p}}{\partial x_i}=0 \quad (6)$$

Eq. (4) expresses conservation of gas mass; Eq. (5), conservation of water mass; and Eq. (6) conservation of momentum. The primary unknowns are: displacement u_i, gas pressure p_g and water pressure p_w. Other equation parameters are defined as follows:

- n is porosity; H is Henry's coefficient of dissolution for gas in water; K_w, K_s, and K_g are the bulk moduli of the water, the solid material and the gas, respectively; and μ_w and μ_g are the viscosity of water and gas, respectively.
- k_{rw} and k_{rg} are, respectively, the relative permeability of water and gas.
- p_c=p_g-p_w is suction; $\bar{p}$ is the maximum value between p_g and p_w so that it becomes the water pressure when the medium is saturated with water, and the gas pressure when a separate gas phase exists.
- S_w is water saturation (the portion of the pore occupied by liquid water).
- α_B is Biot's coefficient.
- C_{ijkl}, the fourth order tensor stiffness tensor was derived from the elastoplasticity framework, taking into account the inherent anisotropy of the rock due to bedding (Nguyen and Le, 2015).

5.2 Stress-strain behaviour of OPA

The stress-strain behaviour of OPA is an important component of the mathematical model previously described and must be understood with reasonable confidence in order to allow a credible simulation of the field experiment c. That stress-strain behaviour is mathematically represented by the stiffness tensor C_{ijkl} in Eq. (6). Nguyen and Le (2014) used existing laboratory triaxial test data on OPA, the host formation for the HG-A experiment, in order define the stiffness tensor, assuming that OPA is elasto-plastic. The resulting stress-strain relationship incorporates the major phenomena which are evidenced from the experimental data:

- Non-linear stress-strain response with irrecoverable strain when the stress level exceeds a certain limit.
- Transverse isotropy due to bedding.
- Time-dependency.

5.2.1 Hooke's law of elasticity for an anisotropic material

In the elastic domain, it is assumed that Hooke's law is applicable. Since OPA is assumed to be transversely isotropic, five independent elastic constants are needed: $E_{//}$, $E_{\perp}$ (the Young's moduli); $\nu_{//\perp}$, $\nu_{////}$ (the Poisson's ratios); and $G_{////}$ (the shear modulus). The subscripts // and $\perp$ respectively denote the direction parallel and perpendicular to bedding. In addition to the consideration of transverse isotropy of the elastic constants, the Young's moduli are also assumed to degrade with time in order to simulate the time-dependent deformation observed in triaxial creep tests. The degradation of the Young's moduli with time is simulated using exponential decay functions, with parameters given in Table 2. These parameters were derived by calibrating finite element models that simulate the laboratory creep tests.

5.2.2 The Mohr-Coulomb yield criterion with strain hardening/-softening

The Mohr-Coulomb yield criterion was adopted. Strain hardening and softening was taken into account by making the cohesion c and friction angle ϕ as functions of the effective plastic strain $\overline{\varepsilon_p}$, defined as:

$$\overline{\varepsilon_p}=\sqrt{\frac{2}{3}\varepsilon_p:\varepsilon_p} \quad (7)$$

Following the approach used by Martin and Chandler (1994), it was assumed that c degrades with thr effective plastic strain while the mobilized friction angle ϕ increases to a maximum value that accounts for interlocking effects before decreasing to a residual value. Based on that observation, the fitting of $c(\overline{\varepsilon_p})$ and $\phi(\overline{\varepsilon_p})$ will be determined based on the initial yield, interlocking and residual points, and the variation of stress-strain curve that are obtained from the triaxial test data. The mathematical expressions are as follows:

$$c(\overline{\varepsilon}_p)=c_0+(c_0-c_r)*\exp(-A\overline{\varepsilon}_p)$$
$$\phi(\overline{\varepsilon}_p)=\begin{vmatrix}\phi_0+\phi_0\sqrt{\overline{\varepsilon}_p/\varepsilon_i} & \overline{\varepsilon}_p\le\varepsilon_i\\ \phi_r+(\phi_i-\phi_r*)\exp(-A\overline{\varepsilon}_p) & \overline{\varepsilon}_p\succ\varepsilon_i\end{vmatrix} \quad (8)$$

where the subscript r denotes the residual state, o denotes the initial state, i denotes the interlocking, ε_i is the strain at which the maximum friction due to interlocking occurs and A_c and A_ϕ are the decay factors calibrated from experimental data from triaxial tests.

A non-associated plastic flow rule is adopted. The plastic flow potential is assumed to take a similar form as the yield function; however, the friction angle is replaced by a dilation angle ψ which is proportional to the friction angle ϕ by a factor varying from 0 to 1.

5.2.3 Modelling the inherent anisotropy of yield parameters using a microstructure tensor approach

Table 2. Input Properties of OPA used in modelling of the HG-A experiment.

Parameters	Variable/Unit	Value
Geomechanical properties (derived from triaxial tests in this paper)		
Young's moduli	$E_{//}$ [MPa]	$2500+3500\mathrm{e}^{(-0.1t/86400)}$
	$E_{\perp}$ [MPa]	$900+2500\mathrm{e}^{(-0.1t/86400)}$
Poisson ratio	$\nu_{////}$ [- -]	0.33
	$\nu_{//\perp}$ [- -]	0.25
Shear modulus	$G_{////}$ [MPa]	1,400
	$G_{//\perp}$ [MPa]	$E_{\perp}/(2*(1+\nu_{////}))$
Cohesion, initial	c_p [MPa]	$\mathrm{c_p} = 2.03\left\{\begin{array}{l} 1+2.536(0.1(1-3l_2^2))+ \\ 40.25(0.1(1-3l_2^2))^2-81.59(0.1(1-3l_2^2))^3 \end{array}\right\}$
Cohesion, residual	c_r [MPa]	$c_r = 0.455\left\{\begin{array}{l} 1+10.480(0.1(1-3l_2^2))+ \\ 68.13(0.1(1-3l_2^2))^2-96.63(0.1(1-3l_2^2))^3 \end{array}\right\}$
Friction angle, interlocking	ϕ_i [°]	$\phi_i = 14.4\left\{\begin{array}{l} 1+0.44(0.1(1-3l_2^2))+ \\ 10.67(0.1(1-3l_2^2))^2-28.44(0.1(1-3l_2^2))^3 \end{array}\right\}$
Friction angle, residual	ϕ_r [°]	$\phi_r = 19.13(1+0.4182(0.1(1-3l_2^2)))$
Dilatancy	Ψ [°]	0.667ϕ
Biot coefficient	α_B [- -]	0.6
Solid density	ρ [kg· m^{-3}]	2,470
Hydraulic properties (based on NAGRA, 2008)		
Porosity	ε_f [- -]	0.16
Liquid water density	ρ_w [kg· m^{-3}]	1,000
Gas density (nitrogen)	ρ_g [kg· m^{-3}]	1.13
Water dynamic viscosity	μ_{w} [Pa·s]	0.001
Gas dynamic viscosity	μ_{g} [Pa·s]	$1.78e^{-5}$
Permeability	$k_{//}$ [m^2]	$k_{g,//} = 2*10^{-20}*k_{rg}*e^{-240\varepsilon_v}*e^{-450\varepsilon_{epe}}$ $k_{w,//} = 2*10^{-20}*k_{rw}*e^{-240\varepsilon_v}*e^{-450\varepsilon_{epe}}$
	$k_{\perp}$ [m^2]	$k_{g,\perp} = 4*10^{-21}*k_{rg}*e^{-240\varepsilon_v}*e^{-450\varepsilon_{epe}}$ $k_{w,\perp} = 4*10^{-21}*k_{rw}*e^{-240\varepsilon_v}*e^{-450\varepsilon_{epe}}$
Van Genuchten parameters (based on Popp et al., 2007; NAGRA, 2008; Xu et al., 2013)		
Residual volume fraction	$S_{w,r}$ [- -]	0.02
α	[m^{-1}]	4e^{-3}
n	[- -]	2
m	[- -]	0.5

The inherent anisotropy of OPA due to bedding results in cohesion and friction parameters that depend on the relative orientation between the stress tensor and the bedding orientation. In order to take this into account, the microstructure tensor approach by Pietruszczak and Mroz (2000) was adopted. These authors introduced a microstructure tensor a_{ij} that is a measure of the material fabric and a generalized loading vector L_i whose components represent the magnitudes of traction vectors on the planes normal to the principal axes of the microstructure tensor. In order to take into account the directional dependence of yielding, the cohesion and friction could be expressed in terms of A_{ij}, a deviatoric measure of the microstructure tensor, and l_i, the unit vector along the direction of the generalized loading vector, as:

$$\begin{aligned} c &= c_0(1+b_0A_{ij}l_il_j+b_1(A_{ij}l_il_j)^2+b_2(A_{ij}l_il_j)^3 \\ &+b_3(A_{ij}l_il_j)^4+\cdots) \\ \phi &= \phi_0(1+b_0A_{ij}l_il_j+b_1(A_{ij}l_il_j)^2+b_2(A_{ij}l_il_j)^3 \\ &+b_3(A_{ij}l_il_j)^4+\cdots) \end{aligned} \tag{9}$$

In the case of a bedded material, there are two principal directions in the bedding plane and one principal direction perpendicular to it. The above equations simplify to:

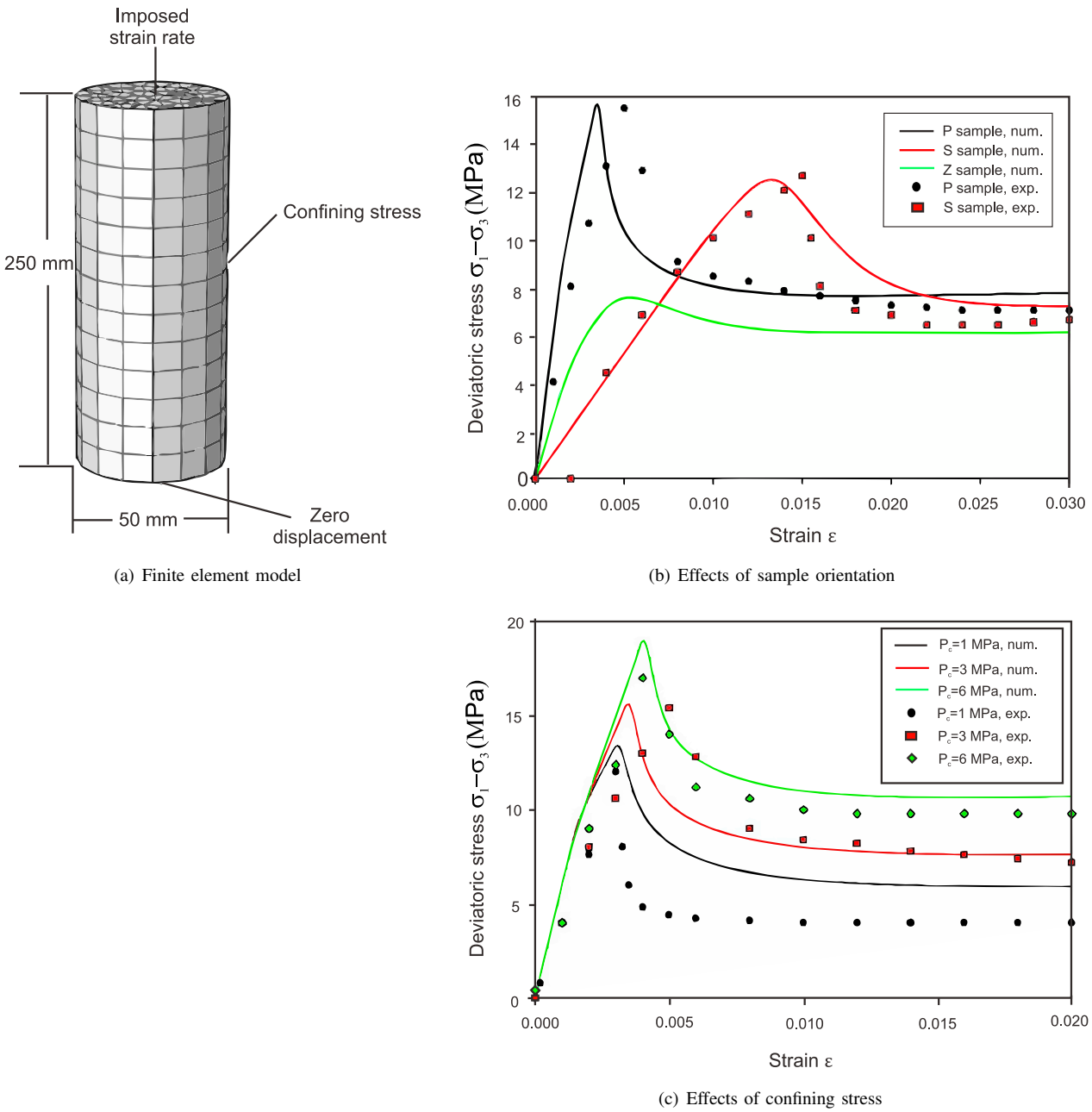

(a) Finite element model

(b) Effects of sample orientation

(c) Effects of confining stress

Fig. 7. Finite element modelling of triaxial tests.

$$
\begin{aligned}
&c = c_0(1 + b_o A_{1,c}(1-3l_2^2) + b_{1,c}(A_{1,c}(1-3l_2^2))^2 + \\
&b_{2,c}(A_{1,c}(1-3l_2^2))^3) \\
&\phi = \phi_0(1 + b_o A_{1,\phi}(1-3l_2^2) + b_{1,\phi}(A_{1,\phi}(1-3l_2^2))^2 + \\
&b_{2,\phi}(A_{1,\phi}(1-3l_2^2))^3)
\end{aligned} \tag{10}
$$

In uniaxial and triaxial tests, the loading direction is related to β, the angle of the bedding plane with respect to the horizontal. For example for uniaxial tests:

$$l_2^2 = \cos^2\beta \tag{11}$$

By using the experimental data from triaxial tests, the expressions of c and ϕ for initial and residual values of cohesion, and initial, interlocking and residual values of friction, are derived as shown in Table 2. Table 2 also lists hydraulic properties of OPA that are used in the simulation of the HG-A experiment, that will be described later.

5.3 Calibration of constitutive model of OPA with laboratory triaxial tests

Triaxial tests for the samples with bedding orientation at 0° (S-sample), 45° (Z-sample) and 90° (P-sample) relative to the axial stress were simulated. The finite element model of a cylindrical sample, 250 mm in length and 100 mm

in diameter is shown in Fig. 7(a). The initial stress in the sample is set to be uniformly equal to the confining pressure. Consistent with the test conditions, a constant strain rate of $10^{-5}s^{-1}$ is prescribed at the top boundary. Zero displacement in all directions is assumed for the bottom boundary, while a constant load equal to the confining pressure is maintained at the circumferential boundary. The input material properties used in the simulation are described previously and given in Table 2, under mechanical properties.

Figs. 7(b) and 7(c) compares the modelling and experimental stress-strain response for samples at different bedding orientations and confining stress, respectively. The modelling results compare favourably with the experimental data by exhibiting many similar features:

- Except for the crack/bedding plane closure zone that is not considered, the model correctly predicts a linear zone, a nonlinear zone before the peak, and a post-peak zone where the strength suddenly collapses to a residual value.
- The modelling results for the peak and residual strength values for the P- and S-samples are in good agreement with the experimental values.
- The model predicts that the P-sample has the highest peak strength, while the Z-sample has the lowest strength. This finding seems to be confirmed by experimental observations reported by Grasle and Plischke (2009), and Abdi et al. (2014).
- Fig. 7(b) shows that the modelled residual strength of all three types of samples is practically independent from the sample orientation. This finding is consistent with the current set of experimental data and with experimental observations summarized by Grasle and Plischke (2009).
- Fig. 7(c) shows the effects of different confining pressures on the stress-strain response for the P-sample. The model results are in general good agreement with the experimental data, with some overprediction of the residual strength for a 1 MPa confining pressure. As expected, peak and residual strengths increase with the confining pressure. The predicted slope of the linear portion of the curves, consistent with the experimental data, is independent of the confining pressure. Although not shown here, the above observations for the effects of confining pressures also apply for the S and Z-samples.

5.4 Numerical simulation of the HG-A experiment

The input parameters of the model, as shown in Table 2, were derived and calibrated with laboratory triaxial tests as previously reported and also laboratory gas injection tests (Nguyen and Le, 2014) for the subsequent simulation of the sequences of excavation, water injection and gas injection of the HG-A experiment. The governing Eqs. (4)-(6) with appropriate initial and boundary conditions were numerically solved using the finite element method. The finite element model is shown in Fig. 8.

The predicted damage zone is shown in the inset of Fig. 9. The effective plastic strain calculated by the model is used in this study as the damage indicator. The modelling results,

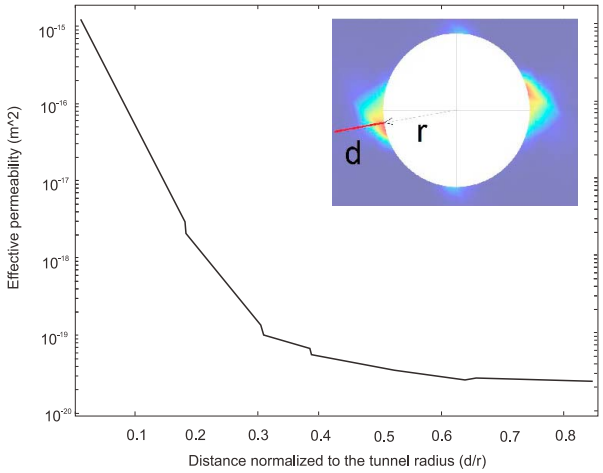

Fig. 9. Excavation damage zone and permeability change.

consistent with the field mapping, show that the main plastic zone develops at locations in between 2 and 3 o'clock and 8 and 9 o'clock. The bedding planes are oriented at 45° with respect to the horizontal axis. The initial in-situ stress is 6.5 MPa in the vertical direction, 2.2 Mpa in the horizontal direction along the tunnel axis, and 4.4 Mpa in the horizontal direction perpendicular to the tunnel axis. The excavation of the tunnel results in a stress redistribution that is dependent on that initial stress state. The shape and extent of the EDZ depends on both that initial in-situ stress and the orientation of the bedding planes. Fig. 9 shows that due to damage, the effective permeability, defined as the geometric mean of the principal components of the permeability tensor, is predicted to increase by up to five orders of magnitude in a zone of approximate thickness of 0.35R (R is the radius of the tunnel). Less significant increases are observed at distances of 0.35 to 0.65R from the periphery of the tunnel. Beyond 0.6R, the permeability remains unchanged. Those predicted trends in the change of permeability are also consistent with observed data.

Fig. 10 shows the calculated evolution of water and gas pressure at different positions in a cross-section of the test tunnel. The numerical results shown in Figure 10 compare favourably with the experimental data at the 12 and 3 o'clock positions in the EDZ. Since the damage zone is more significant at the 3 o'clock position resulting in a high permeability zone, both the gas and water pressures increase more substantially and faster at that position compared to the 12 o'clock position. This indicates that the EDZ, with its higher permeability, is a preferential flow path for both gas and water migration. Therefore, the design and safety assessment of potential DGRs must take into account the EDZ as potential enhanced pathway for radionuclide migration.

Research on rock damage induced by excavation, and how the EDZ can influence water and gas migration is an important activity to provide support to the long-term safety assessment and design of geological repositories for radioactive wastes. Such research must integrate experimental and theoretical developments. In the present example of such research, a mathematical model that couples the stress-strain behaviour

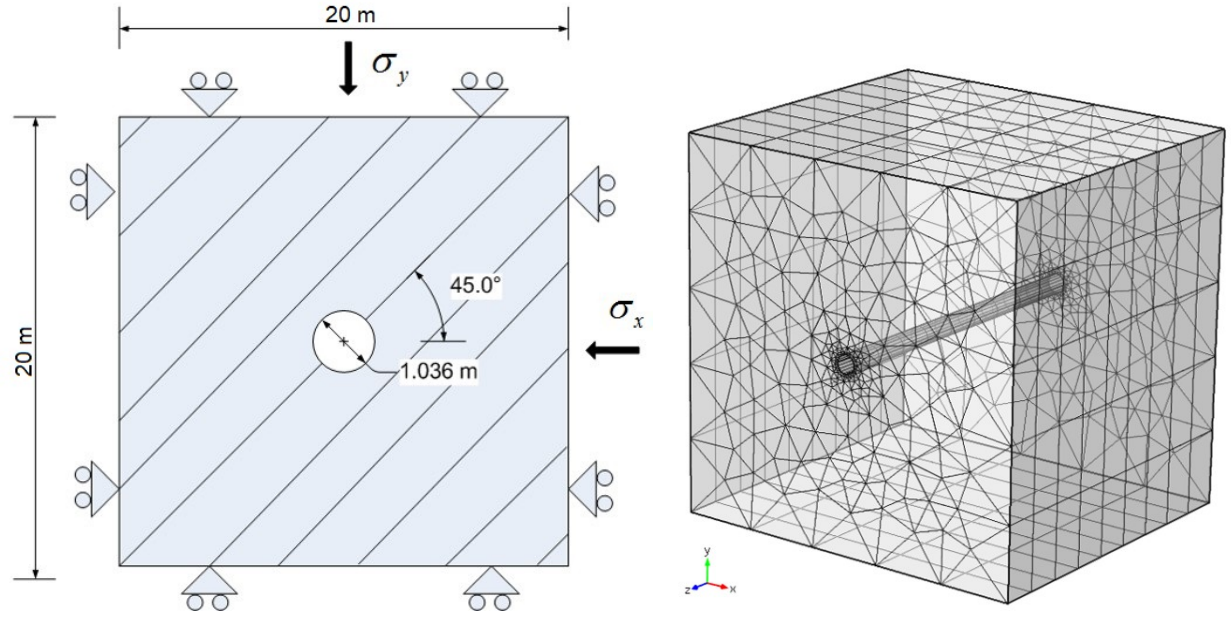

(a) Cross-section showing bedding orientation

(b) 3-D finite element mesh

Fig. 8. Numerical model setup for gas injection test in HG-A experiment.

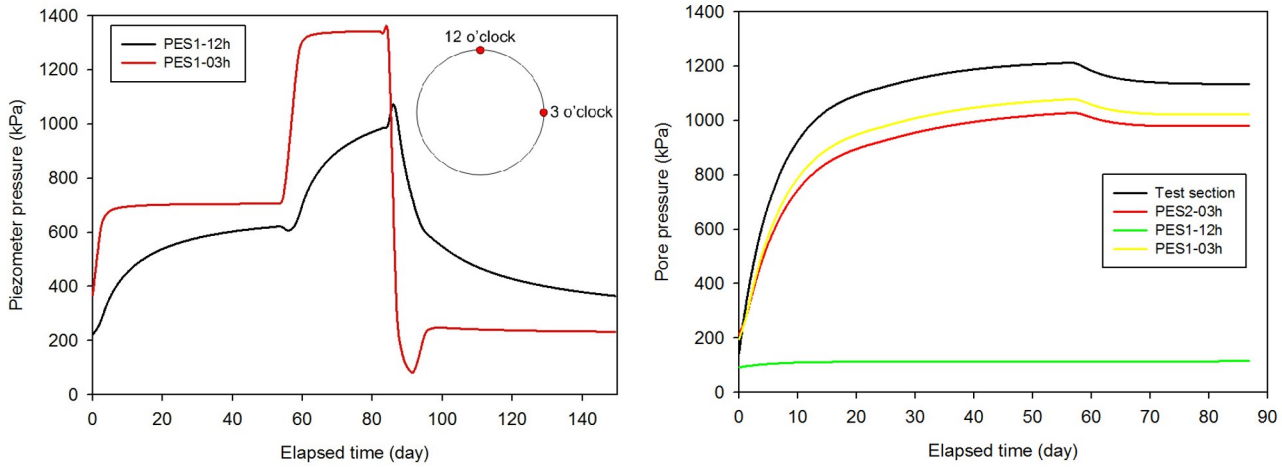

(a) Porewater pressure response to water injection

(b) Gas pressure response to gas injection

Fig. 10. Simulation of pore pressure evolution from water and gas injections.

in the rock mass and two-phase flow transport in the porous media was developed. A fundamental component of the model is the constitutive relationship that governs the mechanical behaviour of the rock, since the success in predicting the EDZ depends on such a relationship. The constitutive relationship that was developed in this research is based on the theory of plasticity with the consideration of inherent anisotropy of sedimentary rock formations, such as OPA. Creep was also considered in the model. That constitutive relationship was included in a mathematical model based on the theory of poromechanics. The poromechanical model was then used to simulate the excavation of the HG-A tunnel in OPA at the Mont Terri URL in Switzerland, followed by water injection and finally gas injection in the tunnel. The good agreement between the predicted and observed hydro-mechanical response of OPA to those sequences shows the robustness of the poromechanical model and the constitutive relationship. In particular, the predicted shape, extent and characteristics of the EDZ are consistent with field observations. The model also predicts that water and gas injected in a test section of the tunnel would preferentially escape into the rock along the EDZ. This prediction is also consistent with the pressure evolution that was observed in the field.

6. Glaciation-induced HMC processes in a sedimentary rock basin

In Canada, sedimentary rocks of the Michigan Basin and crystalline rocks of the Canadian Shield are both currently

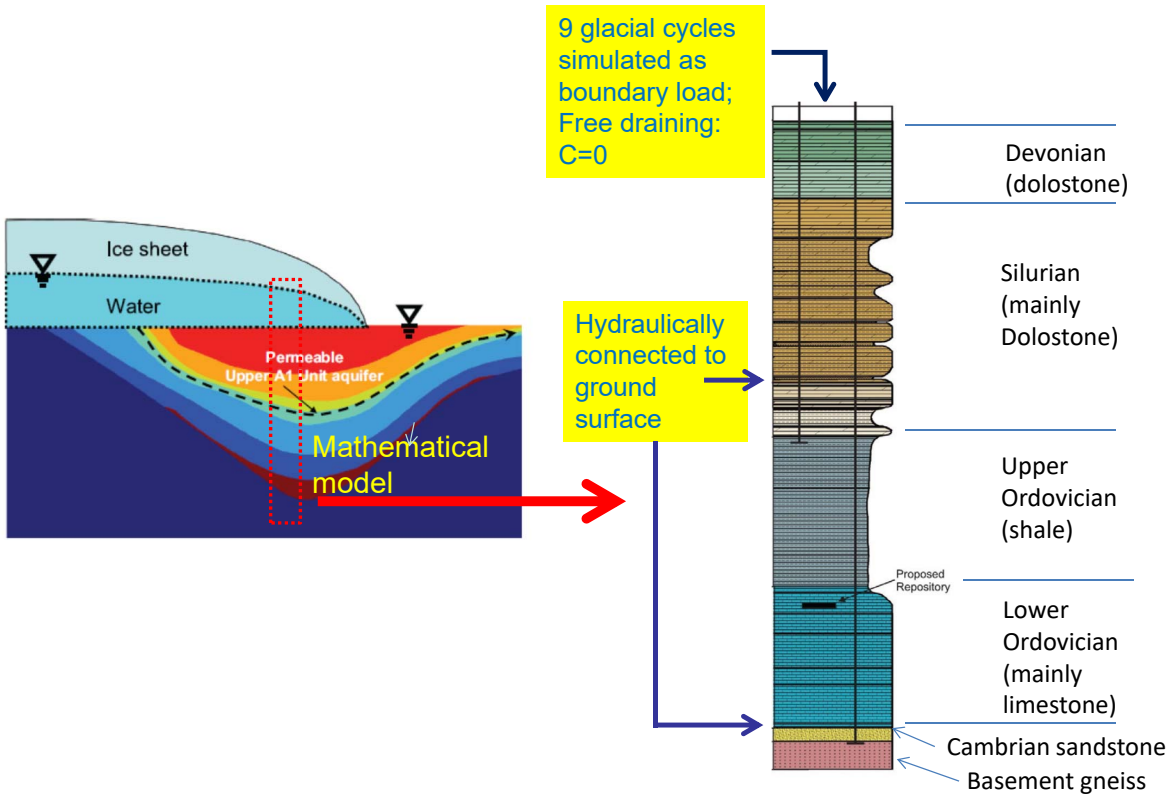

Fig. 11. Conceptual model of continental glaciation of the Michigan Basin.

considered as potential host rock types for the geological disposal of radioactive waste. In this example, we focus on the Michigan Basin sedimentary rocks and look at the HMC processes induced by past and future glacial cycles. Glaciation is a geological event that can generate major perturbations to the THMC regimes in the geosphere, in spatial-temporal scales that are orders of magnitude larger than the ones from any experiment performed at URLs. Sedimentary sequences of the Michigan Basin were deposited onto the Precambrian Shield over several episodes between ~500-300 million years ago. The culmination of the Appalachian orogeny ~250 million years ago was the last major tectonic event to have affected the basin. During the last million years, North America and therefore the region encompassing the Michigan Basin experienced nine glaciation-deglaciation cycles, each one lasting approximately 120,000 years. The last cycle began ~120,000 years ago. At glacial maximum, the maximum ice thickness reached ~4 km, imposing pressures of up to 40 MPa on the surface resulting in depression of the crust by up to 500 m. The advance and retreat of the ice cap resulted in gouging and carving features, including deep valleys, into the bedrock. The Great Lakes began to form ~14,000 years ago at the end of the last glacial period when glacial meltwater filled depressions left behind by glaciers. Geological, hydrogeological and geochemical data gathered from a characterization program performed at the site of a proposed DGR for low and intermediate level radioactive waste (Al et al., 2011) suggest that the deep sedimentary formations around the proposed DGR remain resilient to the past nine glaciation-deglaciation cycles. In this example, we discuss the development of a coupled HMC model to simulate the effects of nine past glaciation-deglaciation cycles on the site of the proposed DGR. The calculated present-day distribution of pore pressure and total dissolved solids' concentrations was compared to the field data. The same model was used to assess the impact of a future similar glaciation-deglaciation cycle on the proposed DGR.

6.1 Governing equations

The mathematical model that was developed to couples mechanical, hydraulic, and chemical transport processes was developed to simulate the nine glacial cycles that occurred over the last million years. The model was formulated using the general framework described in section 2. The governing equations of the model are as follows:

$$\frac{1}{2}C_{ijkl}\left(\frac{\partial^2 u_k}{\partial x_j \partial x_k}+\frac{\partial^2 u_l}{\partial x_i \partial x_l}\right)+\alpha\frac{\partial p}{\partial x_i}=0 \tag{12}$$

$$\frac{\partial (nC)}{\partial t}+\frac{\partial}{\partial x_i}\left(-nD_{ij}\frac{\partial C}{\partial x_j}+V_i C\right)=0 \tag{13}$$

$$\frac{\partial}{\partial x_i}\left(\frac{\rho_w k_{ij}}{\mu}\left(\frac{\partial p}{\partial x_j}+\rho_w g j\right)\right)+\rho_w\left[\frac{-n}{K_w}+\frac{n-\alpha}{K_s}\right]\frac{\partial p}{\partial t}+\rho_w\alpha\frac{\partial}{\partial t}\left(\frac{\partial u_k}{\partial x_k}\right)+n\gamma\frac{\partial C}{\partial t}=0 \tag{14}$$

Eq. (12) is the same equation of equilibrium as Eq. (3). Eq. (13) is the equation of mass conservation for total dissolved solids (TDS), in which C is the TDS concentration. It is assumed that TDS migrates by advection, molecular diffusion and dispersion. V_i is the Darcy's velocity and D_{ij} is the dispersion tensor. Eq. (14) is the equation of porewater mass conservation, similar to Eq. (2) without thermal effects. However, the total dissolved solids concentration C will have an important effect on the water flow process, since it significantly influences the porewater density. It was assumed that the density of the porewater is related to the total dissolved solids through a linear relation:

$$\rho_w = \rho_{w0} + \gamma C \tag{15}$$

In Eq. (14), ρ_w is the porewater density, ρ_{w0} is the porewater reference density, and γ is an empirical constant.

6.2 Numerical simulation results

The conceptual model for the THMC response of the Michigan Basin to continental glaciation is represented in Fig. 11. The conceptual model was implemented in the mathematical model described by Eqs. (12)-(14), with the boundary conditions shown in Fig. 11. Starting at 1 million years before present, the THMC response of the rock formations for one million years was simulated up to the present time. Initially at 1 million years before present, the pore pressure distribution was assumed to be hydrostatic, while the TDS concentration was assumed to follow the profile shown in Fig. 12. That TDS distribution was inferred from paleohydrogeological interpretation discussed in Al et al. (2011).

The input parameters were based on field investigation data (Al et al., 2011) and are summarized in Table 3 for the potential host rock formation (the Cobourg formation) and the surrounding rocks.

The modelling results for the present day distribution of TDS concentration and pore pressure, after nine past glacial cycles, are shown in Fig. 12. The modelling results for TDS concentrations, in good agreement with the field data, show that the deep rock formation is characterized by very dense, saline porewaters that are hundreds of millions of years old. These porewaters have the salinity of brine, with TDS concentration of up to 300 g/l and have remained virtually stagnant despite the tremendous hydraulic and mechanical disturbances induced by the past glaciation cycles. The calculated pressure profile, also in good agreement with the measured data, shows that Ordovician rocks are underpressured relative to hydrostatic conditions. This underpressure was likely due to depressurization after glacial retreat, and subsists to the present time because of very low rock permeability.

It is anticipated that a future glaciation cycle, similar to the ones occurring in the past million years, would start some tens of thousands of years in the future. The same mathematical model was then used to assess the effect of such a future glacial cycle on a proposed DGR (Fig. 13). In Fig. 13, the access shaft (on the left boundary of the model) and the excavated repository are represented by highly permeable features as compared to the rock formations. A conservative (non-sorbing) tracer was distributed in the repository. The tracer concentration is normalized to a value of one at the start of the simulation. Fig. 13(a) shows that due to the future glacial cycle, very large hydraulic pressures and gradients would be induced in the rock formations around the DGR. However the tracer remains confined in the vicinity of the DGR, as shown in Fig. 13(b). A tracer was also distributed in the Cambrian aquifer that overlies the Precambrian basement rock in order to assess the potential for hydraulic connection between the proposed DGR and the Cambrian aquifer. Fig. 13(b) also shows that the tracer would be contained in the Cambrian and no hydraulic connection with the DGR would occur during the next glaciation cycle. Therefore, the model showed that the rock formations would remain resilient to a future glacial cycle and would effectively contain any radionuclides released from the DGR, ensuring long-term safety. Surface water bodies, such as the Great Lakes, would be unaffected.

7. Conclusions

Geological disposal of radioactive waste relies on a multi-barrier system for the long-term protection of humans and the environment. The evolution of the engineered and natural barriers in DGRs for radioactive wastes will influence the long-term safety of the repositories. That evolution is dependent on the coupling between THMC processes that prevail when the barriers are subjected to perturbations. The CNSC has performed experimental and theoretical research on coupled THMC processes since the early 1990s with the collaboration of Canadian and international partners. The CNSC has developed a general theoretical framework that was applied and validated by many experiments. This theoretical framework was implemented in mathematical models that can be used to verify safety arguments for geological repositories proposed in Canada.

THMC processes can occur at different spatial-temporal scales. In this paper we presented examples of processes that can occur in the near-field of the repository as monitored during in-situ experiments performed at underground research laboratories. The spatial and temporal scales of these experiments are respectively of the order of tens of metres and decades. The spatial and temporal scales associated to a DGR are on the other hand, of the orders of kilometers and hundreds of thousands of years. In the last example, the author examined paleohydrogeological information on past continental glaciation, in order to assess the implications of THMC processes on barrier performance at spatial-temporal scales commensurate with the ones for a deep geological repository. The CNSC research is currently continuing in that trend and will focus on the study of THMC processes in natural analogues, such as natural high-grade uranium ore bodies.

Acknowledgements

The author sincerely thanks the CNSC for its funding and colleagues at the CNSC for peer review of this article.

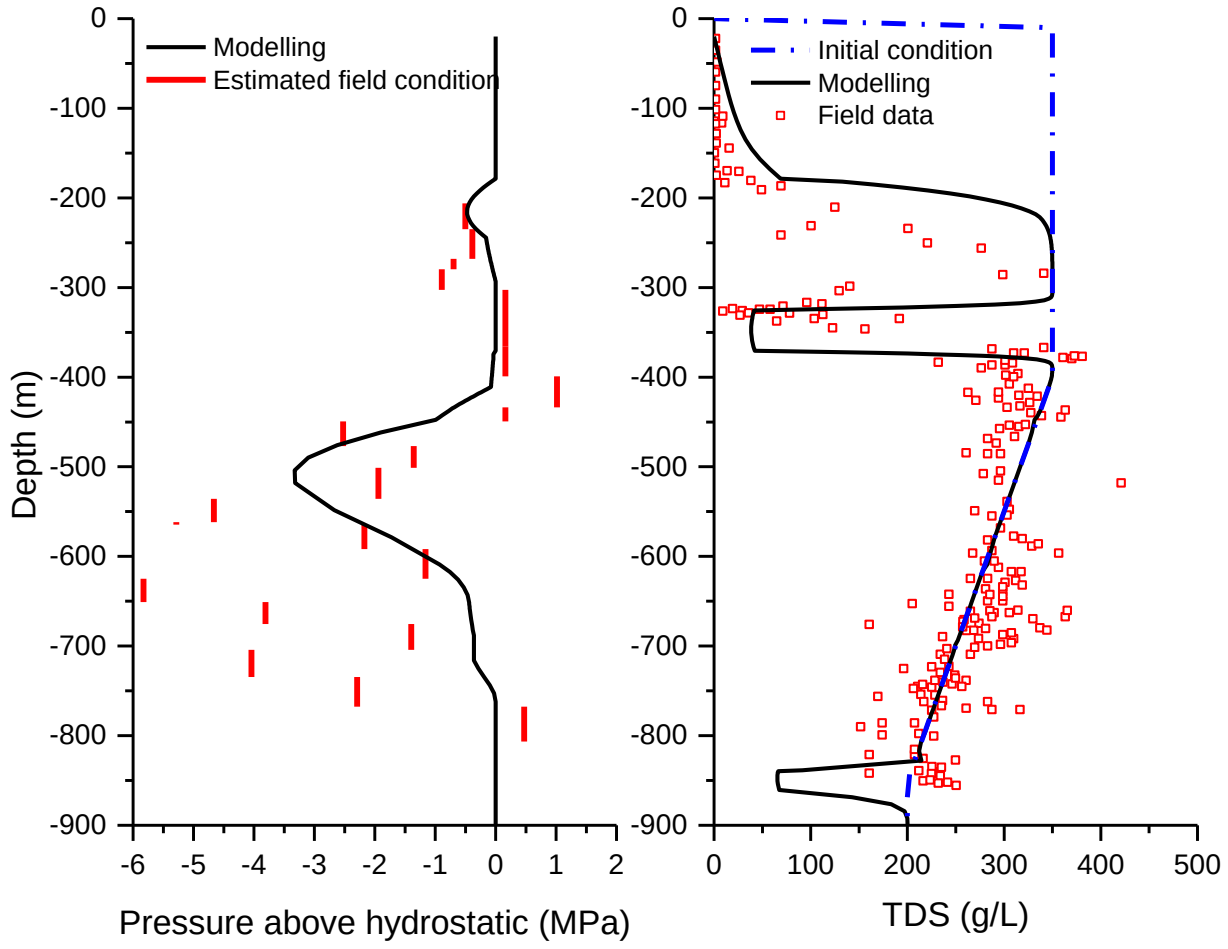

Fig. 12. Present day pressure and TDS concentration profile.

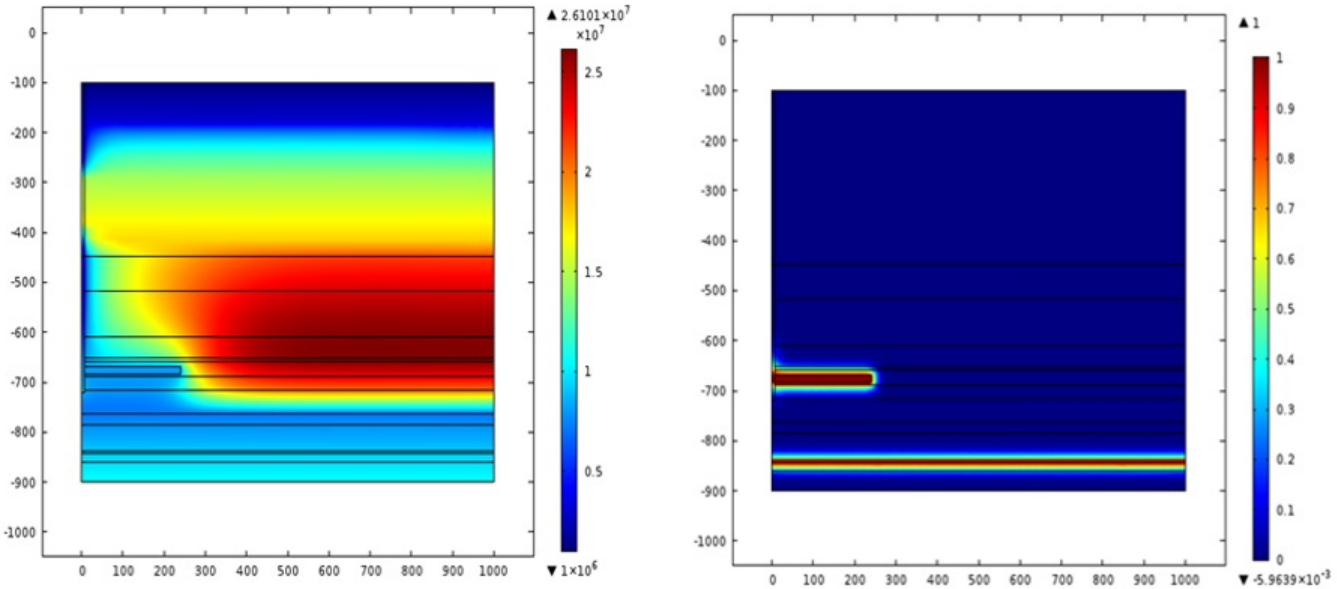

(a) Hydraulic pressure

(b) Normalized tracer concentration

Fig. 13. Effects of future glacial cycle on a DGR.

Table 3. Typical input properties for glaciation modelling.

Depth (m)	Formation name	Hydraulic Conductivity		Porosity (%)	Mechanical parameters		Efective diffusion coefficient (m/ s^2)
		k_h (m/s)	k_h:k_v	%	E (GPa)	v	
447.7	Queenston	3.00E-14	10	7.05	15	0.31	3.60E-12
518	Gorgian Bay	3.00E-14	10	7.1	12	0.23	3.60E-12
608.9	Blue Moutain	3.00E-14	10	7.35	5	0.1	4.30E-13
651.6	Collingwood Member	2.00E-14	10	2.1	30	0.27	4.30E-13
659.5	Cobourg Lower member	1.00E-14	10	1.8	39	0.3	1.10E-13
688.1	Sherman Fall	9.00E-15	10	1.72	23	0.22	1.10E-13
716.1	Kirkfield	4.00E-15	10	1.95	26	0.2	6.90E-13
762	Coboconk	2.00E-11	10-1000	0.75	68	0.33	6.90E-13
785	Gull River	2.00E-12	10-1000	1.95	56	0.27	6.90E-13
838.6	Shadow Lake	1.00E-09	10	1.95	23	0.33	1.00E-10
843.8	Cambrian	3.00E-06	1	8.9	23	0.33	1.00E-10
860.7	Precambrian	1.00E-10	1	3.8	68	0.33	2.20E-12

Participants in the DECOVALEX project (www.decovalex.org) are also particularly acknowledged for many decades of collaboration.

Conflict of interest

The author wishes to confirm that there are no known conflicts of interest associated with this publication and there has been no significant support for this work that could have influenced its outcome.

References

Abdi, H., Labrie, D., Nguyen, T.S., et al. Laboratory investigation on the mechanical behaviour of Tournemire argillite. Can. Geotech. J. 2014, 52(3): 268-282.

Al, T., Beauheim, R., Crowe, R., et al. OPG's Deep Geologic Repository for Low & Intermediate Level Waste-Geosynthesis. Nuclear Waste Management Organization, report NWMO DGR-TR-2011-11, 2011.

Biot, M.A. General theory of three dimensional consolidation. J. Appl. Phys. 1941, 12(2): 155-164.

Bishop, A.W., Blight, G.E. Some aspects of effective stress insaturated and partly saturated soils. Géotechnique 1963, 13(3): 177-197.

Gens, A., Vaunat, J., Garitte, B., et al. In situ behaviour of a stiff layered clay subject to thermal loading: observations and interpretation. Géotechnique 2007, 57(2): 207-228.

Gräsle, W., Plischke, I. Laboratory Testing (LT) Experiment: Mechanical behavior of Opalinus clay, Final report from Phase 614. BGR, Germany, Mont Terri Project Technical Report, 2009.

Le, D., Nguyen, T.S. Hydromechanical response of a bedded argillaceous rock formation to excavation and water injection. Can. Geotech. J. 2014, 52(1): 1-17.

Marschall, P., Trick, T., Lanyon, G.W., et al. Hydro-Mechanical evolution of damaged zones around a micro-tunnel in a claystone formation of the Swiss Jura mountains. The 42nd US Rock Mechanics Symposium (USRMS), San Francisco, California, 29 June-2 July, 2008.

Martin, C.D., Chandler, N.A. The progressive fracture of Lac du Bonnet granite. Int. J. Rock Mech. Min. Sci. 1994, 31(6): 643-659.

Nasir, O., Fall, M., Nguyen, T.S., et al. Modeling of the thermo-hydro-mechanical-chemical response of sedimentary rocks of Ontario to past glaciations, Int. J. Rock Mech. Min. 2012, 64: 160-174.

Nasir, O., Nguyen, T.S., Barnichon, J.D., et al. Simulation of the hydromechanical behaviour of bentonite seals for the containment of radioactive wastes. Can. Geotech. J. 2017, 54(8): 1055-1070.

Nguyen, T.S., Börgesson, L., Chijimatsu, M., et al. A case study on the influence of THM coupling on the near-field safety of a spent fuel repository in sparsely fractured granite. J. Environ. Geol. 2009, 57(6): 1239-1254.

Nguyen, T.S., Le, D.A. Simultaneous gas and water flow in a damage-susceptible bedded argillaceous rock. Can. Geotech. J. 2014, 52(1): 18-32.

Nguyen, T.S., Le, D.A. Development of a constitutive model for a bedded argillaceous rock from triaxial and true triaxial tests. Can. Geotech. J. 2015, 52(8): 1072-1086.

Nguyen, T.S., Li, Z., Barnichon, J.D., et al. Modelling a heater experiment for radioactive waste disposal. Environ. Geotech. 2017, 1-14.

Nguyen, T.S., Selvadurai, A.P.S., Armand, G. Modelling the FEBEX THM experiment using a state surface approach. Int. J. Rock Mech. Min. 2005, 42(5-6): 639-651.

Noronha, J. Deep geological repository conceptual design report-crystalline/sedimentary rock. Nuclear Waste Management Organization, report APM-REP-00440-0015

R001, 2016.

Sevadurai, A.P.S., Nguyen, T.S. Scoping ananalyses of the coupled thermal-hydrological-mechanical behaviour of the rock mass around a nuclear fuel waste repository. Eng. Geol. 1997, 47(4): 379-400.

Terzaghi, K.V. Die berechnung der durchlassigkeitsziffer des tones aus dem verlauf der hydrodynamishen Spannungserscheinungen, akademie der wissenschaften in wien. Mathematish-Naturwissen-Schaftiliche Klasse 1923, 132: 125-138.

Tsang, C.F. Introduction to Coupled Processes. New York, USA, Academic Press, 1987.

Wileveau, Y. THM behaviour of host rock (HE-D) experiment: progress report. Part 1. Mont Terri Project, Technical Report TR 2005-03, 2005.